Available online at www.sciencedirect.com
ScienceDirect
C. R. Physique 10 (2009) 268–282
COMPTES RENDUS PHYSIQUE

Carbon nanotube electronics / Électronique à nanotubes de carbone

Exploring the electronic band structure of individual carbon nanotubes under 60 T

Sébastien Nanot, Walter Escoffier, Benjamin Lassagne [1], Jean-Marc Broto, Bertrand Raquet *

Laboratoire national des champs magnétiques intenses UPR3228, CNRS, INSA, UPS, université de Toulouse, 143, avenue de Rangueil, 31400 Toulouse, France

Available online 26 June 2009

Abstract

Nano-sciences, and in particular nano-physics, constitute a fascinating world of investigations where the experimental challenges are to synthesize, to address (for instance optically or electrically) to explore and promote the remarkable physical properties of new nano-materials. Somehow, one of the most promising realization of nano-sciences lies in carbon-based nano-materials with sp^2 covalent bonds. In particular, carbon nanotubes, graphene and more recently ultra-narrow graphene nano-ribbons are envisioned as elementary bricks of the future of nano-electronics. However, prior to such an achievement, the first steps consist in understanding their fundamental electronic properties when they constitute the drain–source channel of a gated device or inter-connexion elements. In this article, we present the richness of challenging experiments combining single-object measurements with an extreme magnetic environment. We demonstrate that an applied magnetic field (B), along with a control of the electrostatic doping, drastically modifies the electronic band structure of a carbon nanotube based transistor. Several examples will be addressed in this presentation. When B is applied parallel to the tube axis, a quantum flux threading the tube induces a giant Aharonov–Bohm conductance modulation mediated by Schottky barriers whose profile is magnetic field dependent. In the perpendicular configuration, the applied magnetic field breaks the revolution symmetry along the circumference and non-conventional Landau states develop in the high field regime. By playing with a carbon nanotube based electronic Fabry–Perot resonator, the field dependence of the resonant states of the cavity reveals the onset of the first Landau state at zero energy. These experiments enlighten the outstanding efficiency of magneto-conductance experiments to probe the electronic properties of carbon based nano-materials. ***To cite this article: S. Nanot et al., C. R. Physique 10 (2009).***

Résumé

Étude de la structure de bande électronique de nanotubes de carbone isolés sous 60 T. Les nano-sciences, et plus particulièrement la nano-physique, constituent un champ d'investigations aux défis expérimentaux multiples incluant la synthèse, l'adressage (par exemple, optique ou électrique), l'étude et l'exploitation des propriétés physiques remarquables des nano-objets individuels. Les nano-matériaux carbonés (hybridation sp^2) concentrent aujourd'hui une attention toute particulière ; en effet, les nanotubes de carbone, le graphène et plus récemment encore les nano-rubans de graphène pourraient constituer d'ici peu des briques élémentaires de la micro-électronique du futur. Mais en premier lieu, il convient d'insister sur la compréhension des mécanismes de transport

* Corresponding author.
E-mail address: raquet@lncmp.org (B. Raquet).
[1] Permanent address: Laboratoire de physique et chimie des nano-objets, LPCNO URM 5215, 135, avenue de Rangueil, 31077 Toulouse cedex, France.

1631-0705/$ – see front matter
doi:10.1016/j.crhy.2009.05.005

de charges lorsque ces nano-objets sont utilisés comme élément actif du canal drain–source soumis à un potentiel de grille, ou bien comme élément passif pour l'interconnection. Dans cet article, nous présenterons l'intérêt de conduire des expériences où les nano-objets individuels sont soumis à un environnement extrême : l'application de champs magnétiques très intenses et l'utilisation des très basses températures. Nous montrerons que des champs magnétiques de plusieurs dizaines de teslas, associés à un contrôle du dopage électrostatique, modifient singulièrement la structure de bande électronique d'un nanotube de carbone et permettent ainsi de sonder les états électroniques et les spécificités des régimes de conduction associés aux dimensions réduites. Plusieurs exemples seront abordés. Lorsque le champ magnétique est appliqué parallèlement à l'axe du tube, un quantum de flux magnétique pénétrant la section du nanotube engendre une modulation géante de la conductance (de type Aharonov–Bohm), contrôlée par la présence de barrières Schottky dont le profil varie sous champ magnétique. Dans une configuration où le champ magnétique est perpendiculaire à l'axe, ce dernier rompt naturellement la symétrie de révolution et des états de Landau non-conventionels se développent sous fort champ magnétique. En utilisant la sensibilité d'une cavité Fabry–Pérot constituée d'un nanotube de carbone agissant comme un guide d'ondes électronique, il apparaît que les états résonants de la cavité dépendent du champ magnétique transverse. Leurs dépendances révèlent la formation du premier état de Landau à énergie nulle. Ces expériences soulignent l'efficacité des expériences de magnéto-conductance sous champ magnétique intense pour sonder les propriétés électroniques des nano-matériaux individuels à base de carbone. ***Pour citer cet article : S. Nanot et al., C. R. Physique 10 (2009).***

Keywords: Carbon nanotubes; High magnetic field; Electronic conductivity

Mots-clés : Nanotubes de carbone ; Champ magnétique intense ; Conductivité électronique

1. Introduction

Since their emergence in 1991, carbon nanotubes have boosted a fascinating amount of theoretical and experimental work in order to explore, control and promote their outstanding electronic properties relying on a low carrier density, a high mobility and a 1D confinement [1,2]. Even if the road toward microelectronic integration remains challenging, our knowledge of the electronic properties of carbon nanotubes benefits from years of experimental efforts to electrically address individual carbon nanotubes in a controlled manner. Depending on the contact transparency, the presence of the substrate underlying the carbon nanotube, the strength of bias voltage between the drain and the source and also on the electrostatic doping of the tube, the charge transport in a defect-free Single Walled Carbon Nanotube (SWCNT) can manifest itself into very different ways. For instance, by playing with the thickness of Schottky barriers at the contact [3], a same Carbon Nanotube based Field Effect Transistor (CNFET) can behave like an electronic Fabry–Perot cavity [4], a Kondo system for an odd number of electrons in the nanotube [5], or a single electron FET in the Coulomb blockade regime [6]. On the other hand, the voltage-bias conditions on the nanotube can modulate the efficiency of the electronic back-scattering: while low kinetic energy charge carriers are weakly scattered by topologic defects [7] and acoustic phonons [8] near the massless Dirac point, electrons with energies larger than about 160 meV can emit optical phonons, leading to a reduced mean free path [9] and a nonequilibrium phonon distribution [10]. Our understanding of the electronic transport properties of Multi-Walled Carbon Nanotubes (MWCNT) is certainly not so well accomplished. For shells larger than a tenth of a nanometer, the energy separation between the 1D sub-bands becomes comparable to usual bias voltages and the thermal energy at room temperature [2]. The inter-shell coupling is also energy dependent [11]; its impact on the conductance varies with the commensurability between adjacent shells [12] and the drain–source distance [13]. As a consequence, while the conductance versus energy (i.e. the back-gate voltage) curves for SWCNTs are unambiguous fingerprints of their electronic regime, the energy dependence of the conductance for MWCNTs cannot operate alone as a signature of singular events.

For all the aforementioned physical phenomena, an applied magnetic field widely contributes to the exploration of the electronic properties of a carbon nanotube based device. In case of weakly coupled pristine carbon nanotubes to electrodes, the electronic magneto-tunnelling as a function of the back-gate voltage unveils the electronic ground states and the shell-filling [14,15]. Recently, in the McEuen group, a coupling between the spin and the orbital motion of electrons has been demonstrated [16], breaking the widely believed four-fold degeneracy at the charge neutrality point. In case of diffusive MWCNTs, magneto-transport experiments have revealed a unique modulation of the elastic mean free path and the phase coherence length at the vicinity of each van Hove singularity [17]. Most frequently, Kelvin or sub-Kelvin temperatures and DC magnetic fields in the range of few

Tesla are suitable configurations to infer the characteristic energies of charge carriers. However, in this article, we present the usefulness of merging the nano-probing of individual carbon nanotubes and very large magnetic fields, beyond the DC magnetic field limit. After a brief overview of nano-sciences under 60 T and above, we explore the electronic band structure of quasi-ballistic MWCNTs using high field magneto-transport experiments. We demonstrate that the magneto-fingerprint on the conductance is firstly an unequivocal signature of a metallic or a semi-conducting behavior of the external shell. By combining large field and an electrostatic control of the doping, we shed light on unconventional quantum phenomena unique to carbon nanotubes. Under 60 T, threading the carbon nanotube along its axis, the electronic density of states undergoes quantum-flux modulations yielding a giant Aharonov–Bohm oscillation of the conductance, orders of magnitude larger than the standard Aharonov–Bohm effect in metallic rings or cylinders [18,19]. By tilting the magnetic field perpendicular to the tube axis, the symmetry revolution is broken in the high field regime. The magnetic band structure gives rise to unconventional Landau states which can be probed using the sensitivity of a carbon nanotube based electronic Fabry–Perot cavity. Such a measuring scheme allows one to explore the onset of the first Landau state on the circumference of the external shell.

2. Nano-sciences and experiments under 60 T and above

An important trend in modern sciences is the investigation of individually addressed objects with properties determined by a nano-sized group of atoms or molecules. There is an increasing demand from the high magnetic field community to extend single-object measurements up to the highest magnetic fields, to benefit from the powerful combination of nano-sciences and high fields. Indeed, the magnetic length defined by $l_B = \sqrt{\hbar/eB}$ (3 nm at 74 T), becomes comparable to typical dimensions of nano-objects, leading to significant changes in their energy spectrum: the magnetic field drastically lifts the spin and orbital motions of electrons allowing advanced magneto-spectroscopy experiments [20]. When the current flow between electrodes is dominated by weak localization effects due to constructive quantum interference between clockwise and counter-clockwise trajectories, a magnetic length of the order of the size of the nano-object is necessary to gradually destroy the electronic back-scattering [21]. While this phenomenon is commonly used to infer the phase coherence lengths in diffusive conductors, it obviously requires extremely large magnetic fields for nano-scale structures. For free electrons, or those weakly coupled to the lattice, it is also known for a long time that once the magnetic field is higher than the inverse mobility, the motion and the kinetic energies perpendicular to the magnetic field are quantized into Landau states. In case of nano-sized conductors, the Landau states manifest themselves when the first Landau orbit fits into the transverse section of the sample and the electronic system undergoes a transition from a geometrical to a magnetic confinement [22]. In carbon nanotubes, the tubular confinement yields a periodic modulation of the electronic band structure for each quantum flux ($\Phi_0 = h/e$) threading the tube. The required field for a first oscillatory period is $B = 1330\ \mathrm{T/r(nm)^2}$. While thousands of Tesla are necessary for SWCNTs, it falls to 50 T for a 10 nm diameter carbon nanotube. Under a perpendicular magnetic field, the high magnetic field regime occurs once the dimensionless parameter $\nu_B = r/l_B$, becomes larger than one, corresponding to the first cyclotron orbit inscribed on the cylinder surface. Note that $\nu_B^2 = 2\Phi/\Phi_0$, where Φ is the magnetic flux through the tube section $S = \pi r^2$.

The experimental challenge is therefore to extend the single nano-object transport measurements to high magnetic field facilities, well above the DC magnetic field limits, respectively 20, 33 and 45 T for superconducting, resistive and hybrid magnets. The development of pulsed magnetic fields based on the capacitors bank discharge in a resistive coil is an approved technical solution to reach non-destructive 60 T and more [23]. However, to make electronic transport experiments feasible, the key factor is a reasonably long duration of the pulse, in the range of few hundreds of ms. The installation at the LNCMI-Toulouse relies on a crowbar circuit with a 14 MJ capacitors bank of 25 mF, withstanding a maximum charge of 24 kV. Pulses of currents of the order of 20 kA in homemade Zylon/copper coils cooled at the liquid nitrogen temperature ensure routine experiments at 60 T. The implementation of single nano-object measurements in such a high-field facility requires some special cares. Nano-scale samples are usually extremely delicate to handle and can easily be damaged by the aggressive electrical environment inherent to the control of the capacitors bank (see Fig. 1). Specific procedures, shielding and filters are used to safely measure the 60 T magneto-conductance of individual carbon nanotubes, as well as graphene nanoribbons.

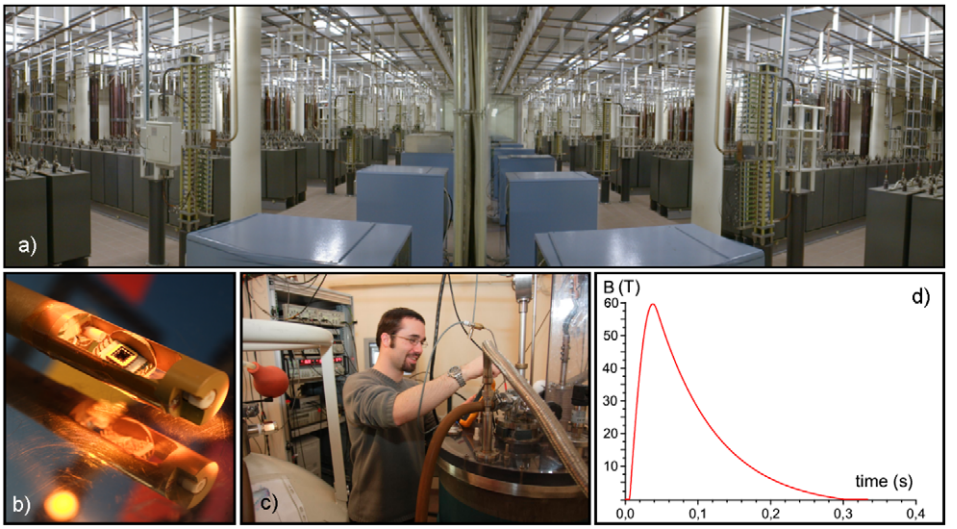

Fig. 1. (a) 14 MJ capacitors bank at LNCMI-Toulouse, France. (b) Photograph of a sample mounted onto a variable temperature insert. (c) Photograph of a 60 T experimental box dedicated to magneto-transport measurements. (d) Typical time evolution a 60 T pulsed magnetic field during a transport experiment.

3. Exploring the electronic band structure of individual carbon nanotubes under 60 T

When we deal with the quantum transport in a mesoscopic system, neglecting the interface effects at the contacts, the Kubo formalism is well suited to estimate the intrinsic resistance [24]. As a first approach, the Kubo conductivity is expressed by: $\sigma = \frac{e^2}{h}\rho\langle D_\varphi\rangle$, where ρ is the electronic density of state and $\langle D_\varphi\rangle$ is the average of the diffusion coefficients of the electronic wave packets. This straightforward expression clearly demonstrates that the electronic transport (and its magnetic field dependence) can be dominated either by peculiarities of the density of states, either by localization effects depending on the degree of disorder and the location of the Fermi energy. This remark sheds light on the long controversy between DoS and localization contributions to the conductance of CNT [25–27,17,21] since the pioneer works of Bachtold et al. in 1999 [28]. These authors gave evidence of the first oscillatory behavior of the conductance on a MWCNT under a 12 T parallel magnetic field. The period equals half the flux quantum and the phenomenon was called Aharonov–Bohm effects for carbon nanotubes. This was the first direct evidence of the major contribution of the external shell since its diameter coincides with the oscillatory period. But on the other hand, the $h/2e$ period is an unambiguous signature of the Altshuler–Aronov–Spivak effect due to constructive interference between trajectories around the circumference in the weak localization regime [29]. In fact, such MWCNTs behave like a standard dirty metallic cylinder with a phase coherence length in range, or larger than the circumference [18]. In fact, a direct spectroscopy of the electronic band structure and its magnetic field dependence by transport measurements requires defect-free carbon nanotube devices with a control of the electronic doping.

3.1. Sample preparation and measurements

Multi-wall carbon nanotubes we work on are first produced by the arc-discharge method, chemically purified and then introduced into an aqueous solution containing surfactant [30]. The latter prevents the formation of carbon nanotube bundles and ensures the presence of free-standing individual nanotubes into the solution. A gentle sonification process also helps to disperse the MWCNT and improves solution homogeneity, just before spreading a drop of it onto a highly doped silicium wafer with a SiO_2 top layer. Pre-fabricated gold micro-electrodes have been patterned on the substrate, which enclose several 500 μm^2 working areas where individual carbon nanotubes are randomly deposited, as the solution progressively evaporates. Following de-ionized water cleaning and drying, atomic force microscopy is used for visualization and localization of the most relevant carbon nanotubes. Several criteria such as length, diameter, relative position and orientation with respect to the electrodes are considered to meet one specific experiment requirement. Then, standard electronic lithography and a lift-off of Palladium nano-electrodes are performed to electrically

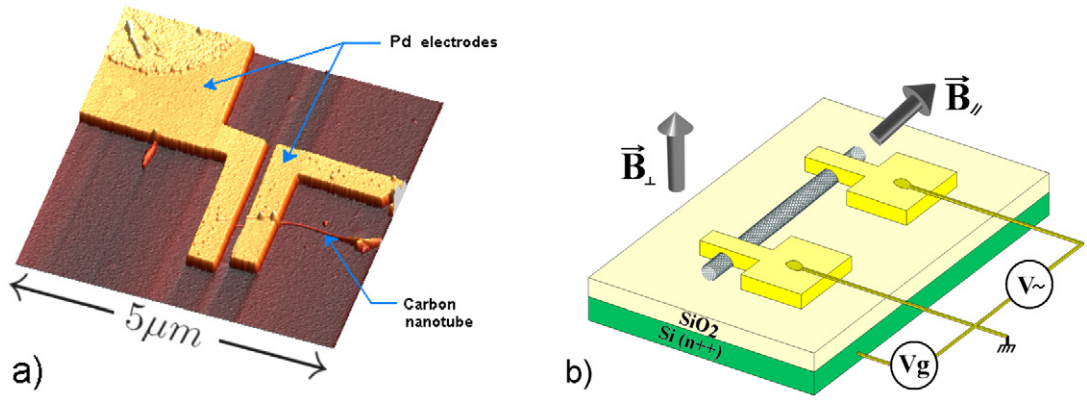

Fig. 2. (a) AFM image of an individually connected multi-wall carbon nanotube of diameter $d = 18$ nm. Pd-electrodes are deposited on the top of the MWCNT. (b) Schematic drawing of the same device. For magneto-conductance experiments, we refer to as the parallel and perpendicular configuration when the magnetic field orientation is, respectively, aligned ($B_{\parallel}$) or normal ($B_{\perp}$) to the nanotube axis.

connect the selected nanotubes to the aforementioned micro-electrodes, which later will connect the sample-holder contact pads. Fig. 2(a) shows AFM image of one MWCNT connected to Pd-electrodes and Fig. 2(b) illustrates the overall design of the CNT-based device. Geometrical parameters such as the inter-electrode distance L_T and the nanotube diameter are extracted from AFM measurements. The Si doped substrate is used as a back gate inducing efficient and controllable electrostatic doping to the device (i.e. the charge carrier density can be continuously changed through the application of a back gate voltage). An ac source–drain voltage is applied to the nanotube while the current flowing through is monitored using lock-in pre-amplifier. The working frequency is chosen above 2 kHz to be compatible with the dynamics of the pulse magnetic field. Upon application of an external magnetic field, such a measuring scheme provides a direct access to the two-probe magneto-conductance of the device. The orientation of magnetic field compared to the nanotube axis can be tilted form 0° to 90° *in situ*, and we shall denote in the following these two extreme situations as the parallel and perpendicular configuration respectively.

3.2. Density of states modulations under 60 T parallel to the CNT axis

In the parallel configuration, the electronic properties of carbon nanotubes are affected by the magnetic field in a rather dramatic and spectacular manner [31,32]. Indeed, as in the case of mesoscopic conducting rings or cylinders, electrons circulating onto the circumference of such hollow systems acquire an additional phase factor directly related to the amount of magnetic flux threading the device cross-section. For a mesoscopic ring, the two trajectories belonging to the two arms develop an opposite phase shift due to the circulation of the vector potential. The electronic transmission is modulated by the phase shift dependence of the interference between the two paths [33]. On the other hand, for CNT, following the Pieirls substitution to account for the magnetic field, the boundary conditions are modified by the vector potential $A(r)$ as follows: $\psi_k(r + C_h) = e^{ik\cdot C_h} e^{\frac{2i\pi}{\Phi_0}\int_{C_h} A(r)\,\mathrm{d}r} \psi_k(r)$, where C_h is the circumference and $\psi_k(r)$ is the electronic wave function. The additional magnetic phase reduces to $2\pi\frac{\Phi}{\Phi_0}$. This causes an uniform shift of the quantized wave-vectors $k_{\perp}$ along C_h, defined by $\Delta k_{\perp} = \frac{2\pi}{C_h}\frac{\Phi}{\Phi_0}$, see [31,32]. As a consequence, the application of a magnetic field leads to a periodic modification of the one-dimensional electronic band structure [34,35], and such an outcome can be directly addressed through magneto-conductance experiments. Despite showing Φ_0 periodic structures, the amplitude and fine details of the magneto-conductance depends on many parameters where temperature, contact transparency and disorder are just a few examples. This effect also strongly depends upon the Fermi energy position within the complex band structure of one particular carbon nanotube. Actually, one of the key mechanisms in conductance modulations lies in the successive opening and closing of an energy gap E_g as a function of magnetic field, together with the splitting and the displacement of the van Hove singularities (vHs) $E_i^{\pm}$ of the density of states. The sign (+) (respectively (−)) is associated with the clockwise (anticlockwise) electron motion around the axis and an orbital magnetic moment antiparallel (parallel) to the applied magnetic field. Depending on chirality, metallic or semi-conducting carbon nanotubes are affected in a different way but the magneto-conductance

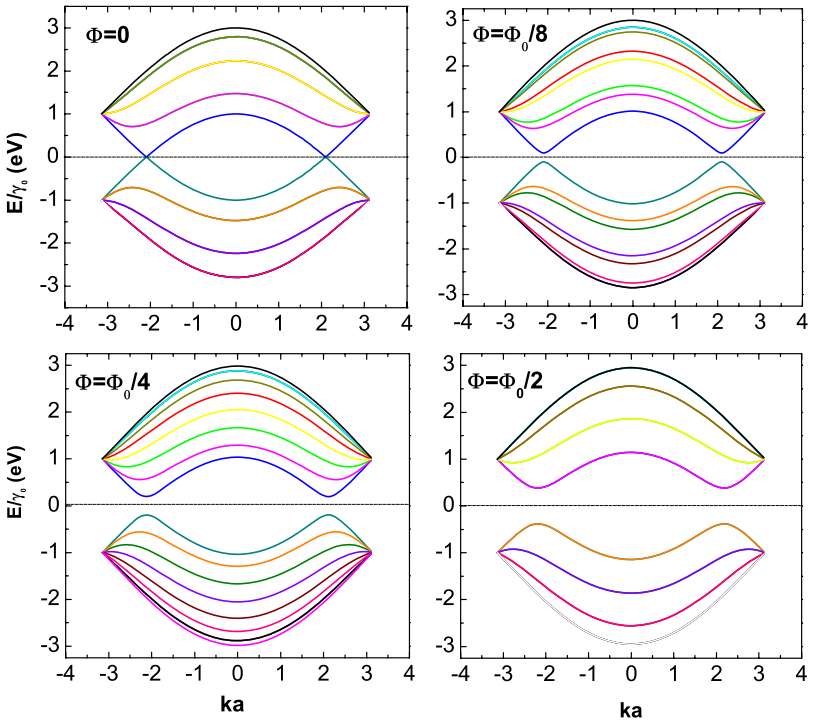

Fig. 3. Electronic band structure of a (10, 10) armchair CNT under different magnetic flux (0, $\Phi_0/8$, $\Phi_0/4$ and $\Phi_0/2$) deduced from the tight binding calculation.

evolution always remains Φ_0 periodic in essence. For instance, in the case of a (10, 10) armchair carbon nanotube, the flux dependence of the electronic band structure deduced from the tight binding calculation is illustrated in Fig. 3. The energy gap and the vHs are expressed by [34]:

$$E_g = 3\Delta_0\Phi_r \quad \text{and} \quad E_i^{\pm} = \gamma_0 \sin\left[\frac{\pi}{n}(i \pm \Phi_r)\right] \tag{1}$$

with

$$\Phi_r = \begin{cases} \Phi/\Phi_0 & \text{if } 0 \leqslant \Phi \leqslant \Phi_0 \\ 1 - \Phi/\Phi_0 & \text{if } \Phi_0/2 \leqslant \Phi \leqslant \Phi_0 \end{cases}$$

Here, $\Delta_0 = 2\gamma_0 a_{cc}/d$, where γ_0 is the energy overlap integral between carbon atoms, a_{cc} is the nearest carbon–carbon atom distance and n the chirality index. We note that such a Φ_0 periodic band structure modulation of a MWCNT has experimentally been reported in the Coulomb blockade regime [36] whereas in SWCNT, manifestations of the Aharonov–Bohm beating effect have been inferred through a detailed analysis of the resonant states of a CNT based Fabry–Perot cavity [37]. Also, optical magneto-spectroscopy under high magnetic field and performed on a collection of SWCNT has revealed a red shift along with the splitting of the vHs in consistency with the Aharonov–Bohm effect [20].

In the following, we shall focus on a 10 nm diameter multi-wall carbon nanotube of length $L_T = 200$ nm between the contacts (see Fig. 2(a)). Preliminary experiments in zero magnetic field and low temperature support the quasi-ballistic nature of the device (not shown here). The two-probes conductance is of the order of $1G_0$, where $G_0 = 2e^2/h$ is the conductance quantum including the spin degeneracy, and weakly changes for a broad range of temperature from 300 K to 4.2 K. The conductance at 100 K does not evolve much when the back gate voltage is swept from $V_g = -20$ V to $V_g = +20$ V, while at low temperature, the conductance versus energy develops quasi-periodic oscillations, signature of Fabry–Perot interference (see next section). As developed further, the application of a strong magnetic field can be used to determine the metallicity of the external shell and to unambiguously set the Fermi energy location with respect to the charge neutrality point.

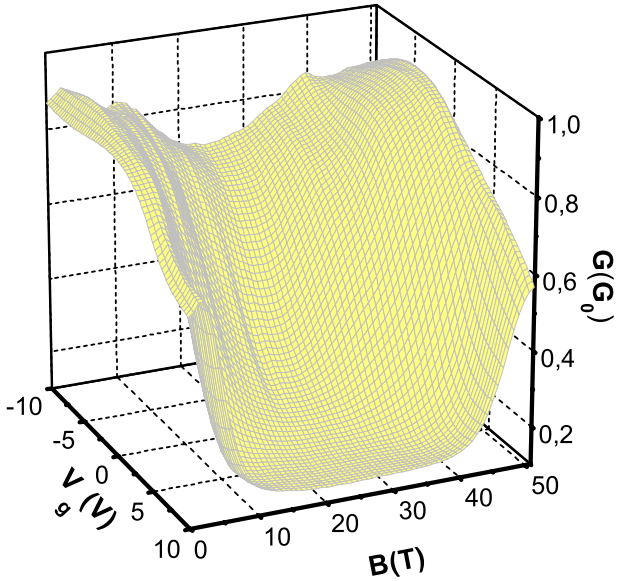

Fig. 4. 3D representation of $G(B, V_g)$ at 100 K. Note the weak magnetic field dependence of the conductance at $V_g = -10$ V, which develops onto a significant U-like curve at the charge neutrality point approaching $V_g \approx +10$ V. For this back-gate voltage, the conductance is magnetically switched off between 18 T and 30 T.

Fig. 4 shows a comprehensive 3D plot of the carbon nanotube conductance as both magnetic field and back gate voltage vary, at fixed temperature $T = 100$ K. For $V_g = -10$ V, a weak decrease of the conductance is first observed at moderate magnetic field before turning into an increasing one, thus describing a weak cusp-like curve showing a minimum at $B^* = 24$ T. Upon increasing the gate voltage, the magneto-conductance remains similar in shape but its relative variations are more and more pronounced, towards developing a large plateau at $G = 0.13G_0$ for $V_g = +10$ V. The vanishing (or increasing) conductance can straightforwardly be explained in terms of a magnetic field induced energy gap opening (or closing) in which, assuming a simple flat-band regime, electrons enter and exit the system by thermal activation. As the Fermi energy is centered or shifted relative to the energy gap, the effect is enhanced or weakened respectively. As mentioned earlier, magneto-conductance oscillations of period $B \approx 50$ T would be observed for a 10 nm-diameter nanotube through the Aharonov–Bohm effect. Experimentally, we note that the full set of $G(B)$ curves appear symmetric and centered around B^*, suggesting a 48 T periodic behavior in fair agreement with theoretical expectations. It is assumed that the most external shell of the MWCNT under study, directly connected to the metallic electrodes, conducts predominantly charge carriers and accounts for most of the effect, although a weak contribution from the inner shells can be responsible for non-zero conductance in the plateau region. Based on the above analysis, we infer an intrinsic p-doping of the system, which is presumably due to electronegative adsorbates (mainly oxygen) on the CNT and its contacts [39]. The charge neutrality point is reached for V_g approaching 7–10 V, where the AB conductance modulations are the strongest in amplitude.

Although this simple model describes qualitatively well the magneto-conductance evolution, a quantitative agreement is desirable to properly evidence the Aharonov–Bohm effect in carbon nanotubes. For this purpose, the flat-band regime is now abandoned in favor of a more realistic model including the formation of a Schottky barrier (SB) at the interface between the nanotube and the electrodes [38,40]. In fact, the combination of the field induced gap opening with the shift of the Fermi energy mediated by V_g necessarily yields to a band bending at the contact. This results in a supplementary magnetic field dependence of the electronic transmission at the contacts. Assuming a ballistic regime, the multi-channel Landauer conductance is therefore expressed by [38]:

$$G(\Phi, \Delta E_F) = \frac{2e^2}{h} \sum N_i \int\limits_{E_i^{\pm}(\Phi)} T_{\text{tot}}(E) \frac{\partial f(E - \Delta E_F)}{\partial E} \, \mathrm{d}E \tag{2}$$

where $T_{\text{tot}}(E)$ is the total transmission coefficient, $f(E)$, the Fermi–Dirac distribution and N_i the number of conduction channels. The locations of the sub-bands $E_i^{\pm}(\Phi)$ are defined by Eq. (1). For simplicity, we assume that the

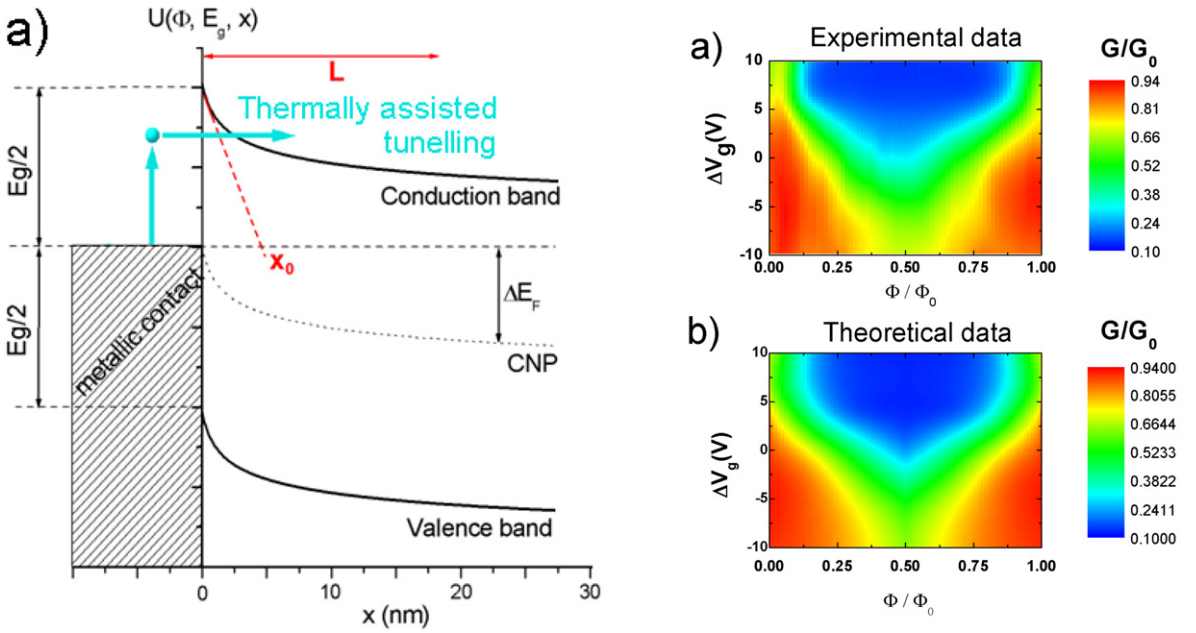

Fig. 5. (a) Schematic diagram of the magnetic field induced Schottky barriers forming at the interface between metallic electrodes and carbon nanotube. (b) Color map representation of $G(B, \Delta V_g)$ constructed from experimental data and (c) using the theoretical expression Eq. (2) with the L and x_0 parameters summarized in Table 1.

barrier height is half the energy gap of the nanotube at $\Phi = \Phi_0/2$, i.e. we neglect the different work functions between the CNT and the Pd-electrodes, so that, no band bending occurs at the charge neutrality point. In the doped states, SB develop at the interface along with the magnetic field induced opening of the energy gap. The band bending is approached by a logarithmic dependence and the potential energy $U(x)$ is written [41]:

$$U(x) = \Delta E_F \left[\frac{\ln(\frac{x_0}{C})}{\ln(\frac{L+x_0}{C})}\right]\left[\frac{\ln(\frac{L+x_0}{C})}{\ln(\frac{x-x_0}{C})} - 1\right] + \frac{E_g}{2} \tag{3}$$

Here, x_0 defines the thickness of the potential profile at the interfaces, L is the penetration width of the barriers and C defines the length unit (see Fig. 5). In this regime, charge carriers enter or exit the nanotube by thermally assisted tunnel processes which directly affect the transmission coefficients T_1 and T_2 of the source and drain barriers respectively. Assuming that incoherent tunnelling takes place at 100 K, the total transmission coefficient $T_{\text{tot}}(E)$ writes $T_{\text{tot}} = T_1T_2/(T_1 + T_2 - T_1T_2)$ [44]. For simplicity, we suppose $T_1 = T_2 = T$. The transparency of the barriers is described through the WKB approximation:

$$T(E) = \exp\left(-2\int_{x_1}^{x_2}\sqrt{\frac{2m^*[U_{(x)} - E]}{\hbar^2}}\right) \tag{4}$$

where x_1 and x_2 are, respectively, the entry and exit point of the barrier and m^* is the effective mass within the CNT.

The magnetic field is taken into account semi-analytically and modulates the transmission coefficient by changing the effective mass m^* as well as the barrier profile $U(x)$. From a straightforward calculation, it can be shown that $m^*(\Phi_r) = 4\pi\hbar^2\Phi_r/(\gamma_0 a_{cc}^2 9n)$ and the magnetic field affects the energy gap $E_g(\Phi_r)$ through Eq. (1). x_0 and L are considered as adjustable parameters and we relate the Fermi energy shift against V_g by standard back-gate coupling $\Delta E_F = \frac{C_g}{C_{\text{elec}}} e\Delta V_g$, where C_{elec} and C_g are the electrochemical and geometrical capacitance respectively. For our typical system dimensions and geometry, we found ΔE_F (meV) $\approx (7 \pm 0.5)(V_g - V_{\text{CNP}})$. In Fig. 5(b), the full experimental curves are plotted in a false color map and compared to the above mentioned model (Fig. 5(c)) with the calculation of the conductance from Eq. (2). An excellent agreement is obtained over the full back-gate voltage and magnetic field range. The corresponding band bending parameters x_0 and L are reported in Table 1. When the Fermi

Table 1
Schottky barrier features and Fermi energy shift at $\Phi = \Phi_0/2$.

$Vg - V_{CNP}$	L (nm)	x_0 (nm)	ΔE_F (meV)
−20	3	1	140 ± 5
−15	5	1	110 ± 5
−10	25	1.2	80 ± 5
−6	60	5	40 ± 5
−4	84	10	30 ± 5
0	flat band	flat band	0

energy shift is small, the SB extend over several tens of nanometers, of the order of the oxide thickness. For larger Fermi energy shift, the barriers become much thinner, in the range of the CNT diameter, and tunnelling is the key mechanism for charge carriers injection through the contacts.

To summarize, the experimental study reported above highlights the fact that, beyond observing Φ_0-periodic modulations of the conductance in a ballistic MWCNT, the results clearly unveil the formation of magnetic field dependent Schottky barriers features between the metallic electrodes and the carbon nanotube. Their establishment is a consequence of a field induced energy gap $E_g(\Phi_r)$ which develops through the Aharonov–Bohm effect. We would like to point out that the quasi-ballistic character of our system has made possible the observation of density of states related effects mainly, in contrast to disordered systems where weak localization associated with $\Phi_0/2$ periodic conductance modulations dominates [42].

In order to go further into the study of sub-band modulation by the Aharonov–Bohm flux within the nanotube, we extend our study to measurements on a larger diameter nanotube ($d = 18$ nm) with a distance $L_T = 150$ nm between contacts (AFM observation). In this case, we expect to observe more than 3 modulation periods within 55 T. Meanwhile, a thinner oxide thickness ($t_{ox} = 40$ nm) is used to enhance the gate efficiency and allow higher doped regime. As shown in Fig. 6(b), the pulsed field magneto-conductance exhibits three periods and a π-dephasing of the modulation when changing the gate voltage. The period of 17 T corresponds to a quantum flux threading a 17.3 nm diameter cylinder, in consistence with the AFM estimation.

The data are directly compared to the conductance calculation based on Eq. (2) for a metallic $(219, 0)$ nanotube (Fig. 6(c)) at 100 K. We assume a ballistic regime and, for a first qualitative approach, SB are neglected. Without any fitting parameter, the agreement between the experimental curves (Fig. 6(b)) and the modelling based on the band structure modulation (Fig. 6(c)), even in the highly doped states where several bands are carrying the current, is convincing. When changing the gate voltage from +10 V to −10 V, successive weakening and π-phase change of the magneto-conductance are experimentally observed. Interestingly, the holes and electrons energies can be deduced at any gate voltage without any analytical estimation by directly comparing the (magnetic) phase and relative amplitude of the effect to the calculated curves. In fact, while the magnetic flux induces successive gap opening and closing, sub-bands at higher energies are split and shifted to lower (E_i^-) (or higher, E_i^+) energies depending on their clockwise (respectively counter-clockwise) movement with respect to the applied magnetic field as shown on Fig. 6(a) [43]. As a consequence, at a given energy, the number of sub-bands carrying the current is modulated. When the Fermi energy is between the CNP and $E_1/2$ (0 and 35 meV in our case, red curves – Fig. 6(b) and Fig. 6(c)), the number of sub-bands passes from 2 to 0 during the first half-period and then rises back to 2 during the second half-period. The magneto-conductance is firstly negative and then positive. At the same time, the magnitude of the oscillations decreases as the Fermi energy increases, and vanishes at $E_F = E_1/2$ where the number of sub-bands is magnetic field independent (green and cyan curves). Between $E_1/2$ and E_1 (35 and 70 meV, black curve), the first van Hove singularity splitting to lower energies induces first an increase of the number of sub-bands from 2 to 4 before $\Phi_0/2$ and then returns to 2 between $\Phi_0/2$ and Φ_0. This corresponds to a π-dephasing compared to the magneto-conductance at low energies. A new vanishing, followed by a new dephasing, is consistently observed when the Fermi energy reaches and goes beyond the first vHs at E_1 (magenta and blue curves). Finally, we conclude that the magneto-fingerprints of the Aharonov–Bohm effect is an unique tool to both identify the metallic or semi-conducting behavior of the external shell and to assign the location of its charge neutrality point and the van Hove singularities. In the present case, the CNP is located at $V_g = 4$ V and the higher sub-bands are located at −2 V, −8 V, and 10 V. We infer an effective gate efficiency of 15 meV/V within the metallic sub-bands. The straightforward calculation of the gate coupling ($\frac{C_g}{C_{elec}}e$) gives a similar value, assuming an oxide thickness of 70 nm, instead of 40 nm. The over-estimate is likely due to the

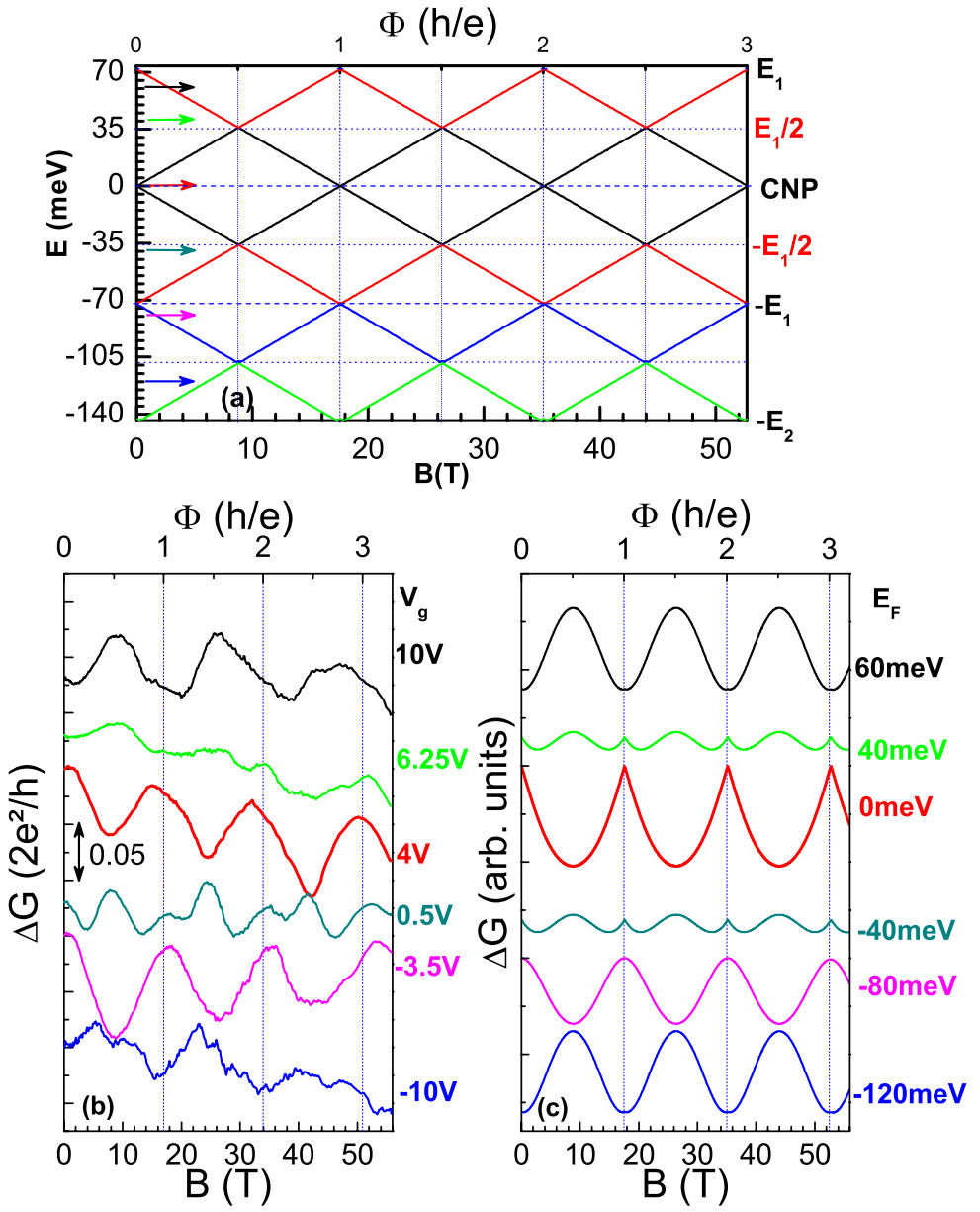

Fig. 6. (a) Magnetic flux dependence of the van Hove singularities following Eq. (1). (b) Experimental magneto-conductance measured on a 18 nm diameter MWCNT (AFM estimate) at 100 K, for various back-gate voltages. Curves are shifted for clarity. (c) Calculation of the magneto-conductance from Eqs. (1) and (2), for a (219, 0) nanotube with different locations of the Fermi energies. Comparison between the experimental and calculated curves yields a direct assignment of the locations of the CNP and the vHs.

screening of the electric field by the large metallic contacts distanced by 150 nm only. Further studies are in progress to understand the small magnitude of the magneto-conductance we measure (0.1G0). An electrical shunt by the inner shells might be considered even if no signature of their contributions is observed on the oscillatory behavior under magnetic field.

3.3. Evidence for Landau states formation in carbon nanotubes

Just recently, little was known on the other configuration, an applied magnetic field perpendicular to the carbon nanotube axis. An analogy with the magnetic band structure recently evidenced in graphene [45–47] is tempting since

a carbon nanotube and graphene have in common their low-energy massless electronic dispersion at the K and K' points of the Fermi surface. Intuitively, one may expect that in the high magnetic field regime, when the first Landau radius is small enough to fit onto the bottom and the top of the tube, the transport properties of the CNTs should mimic those of a graphene flake, irrespective to its semi-conducting or metallic electronic structure. On the other hand, the normal projection of the magnetic field vector onto the tube's wall is non-uniform, the revolution symmetry is broken but the total magnetic flux threading the unit cell defined by C_h and T, the translational vector, is always zero [48]. As a consequence, the transverse vectors are no longer good quantum numbers while the translational symmetry along the axis is preserved. Calculations based on the $\vec{k} \cdot \vec{p}$ theory [31,32] and supersymmetry arguments [49,47] predict a flattening of the one-dimensional sub-bands when the magnetic length l_B approaches the nanotube radius ($\nu_B \approx 1$). The strong reduction of the Fermi velocity at the K and K' points depicts the electronic localization of non-propagating Landau-like states. However, for energies far from the corners of the hexagonal Brillouin zone, the magnetic sub-bands remain dispersive [48] and snake-like currents are predicted to develop at the flanks of the nanotube [47,50]. Note that in the extreme case, when a quantum flux threads the hexagonal carbon cell (for a magnetic field in the range of 80 000 T!), the electrons coupled to the lattice exhibit a pseudo-fractal energy spectrum with aperiodic modulations of the DoS at the CNP [48,50]. However, those phenomena are far above the currently accessible magnetic fields.

Consequences on the electronic transport are certainly not straightforward. On pristine tubes, the reduction of the group velocity of electrons exactly compensates the enhancement of the DoS, so the conductance ought to be unchanged at the CNP. For higher energies, the vHs of the massive sub-bands shift towards higher energies along with the formation of the Landau states. A higher electrostatic potential is therefore required to gain an extra conducting channel [50,51]. If one introduces an Anderson-like disorder, the magnetic field is supposed to induce a large re-introduction of the electronic back-scattering, accompanying the enhancement of the DoS [52]. These theoretical simulations crucially suffer from a lack of experimental evidence. Recent transverse magneto-conductance on clean single-walled carbon nanotube have been performed in the range of $(l_B/r)^2 \sim 0.1$, clearly too weak to form Landau states [40]. Other works on MWCNTs unveiled a diffusive regime with quantum correction to the classical conductance. The positive magneto-conductance mediated by the presence of vHs was assigned to the suppression of the weak localization, following the standard 1D behavior, but with no hint of Landau states formation [17]. Our experimental approach is therefore twofold: (i) to work on clean and quite large MWCNTs to favor density of states fingerprints on the conductance in the high field regime; and (ii) to magnify such fingerprints by playing with a carbon nanotube based Fabry–Perot cavity. As it has been aforementioned, the conductance at the CNP on defect-free tubes is magnetic field independent despite the formation of the zero energy Landau state. With a Fabry–Perot cavity, we expect an enhanced sensitivity of the magnetic field modulation of the electronic transmission through the cavity as a consequence of the field dependence of the resonant longitudinal $k_{\parallel}$-vectors accompanying the flattening of the metallic bands.

Fig. 7(a) shows the differential conductance versus the energy for a 10 nm diameter MWCNT with a small drain–source distance ($L_T \approx 220$ nm), at three temperatures (124 K, 12 K and 2 K). The low-temperature curves exhibit large and quasi-periodic modulations. The average conductance is centered at $1G_0$. The zero energy location has been assigned from the giant Aharonov–Bohm modulation of the energy gap measured on the magneto-conductance under a parallel magnetic field (similar results to those presented in the previous section, not shown here). The back-gate efficiency through a 350 nm SiO_2 oxide is estimated to 2.6 meV/V. Our experimental energy window remains centered on the metallic bands of the MWCNT. Interestingly, such conductance modulations are very robust to several thermal cycles over weeks and their Fourier transform gives a main oscillatory period of 7.5 meV. This period agrees with the expected one in the open quantum dot regime defined by $\Delta E = h v_F/2L_T$, with a Fermi velocity of 8×10^5 m s^{-1} [4]. The maxima of conductance are therefore assigned to the resonant states of the cavity defined by $2L_T \times k_{\parallel} = 2\pi \times n$. In other words, the transmission of the cavity is optimal each time constructive interferences develop between incoming electronic wave-packets and those having experienced a full round trip between the electrodes. Simulation of the conductance versus the energy has been performed in the frame of the Landauer–Büttiker formalism [53]. Semi-reflecting contacts have been considered and an Anderson disorder is introduced to account for an electronic mean free path of the order of the tube length, in agreement with the average $1G_0$ conductance of the tube. The simulation exhibits large Fabry–Perot oscillations smeared by the presence of disorder. Both their magnitude and period are very similar to our experiment. The magnetic field dependence of the electronic transmission through the CNT-based cavity is illustrated in Fig. 7(c), for distinct energies ranging from a resonance at $E = 7$ meV to the nearest out of resonance at $E = 10$ meV. We first remark that the zero-field resonant state at $E = 7$ eV (black curve) starts switching to the off-

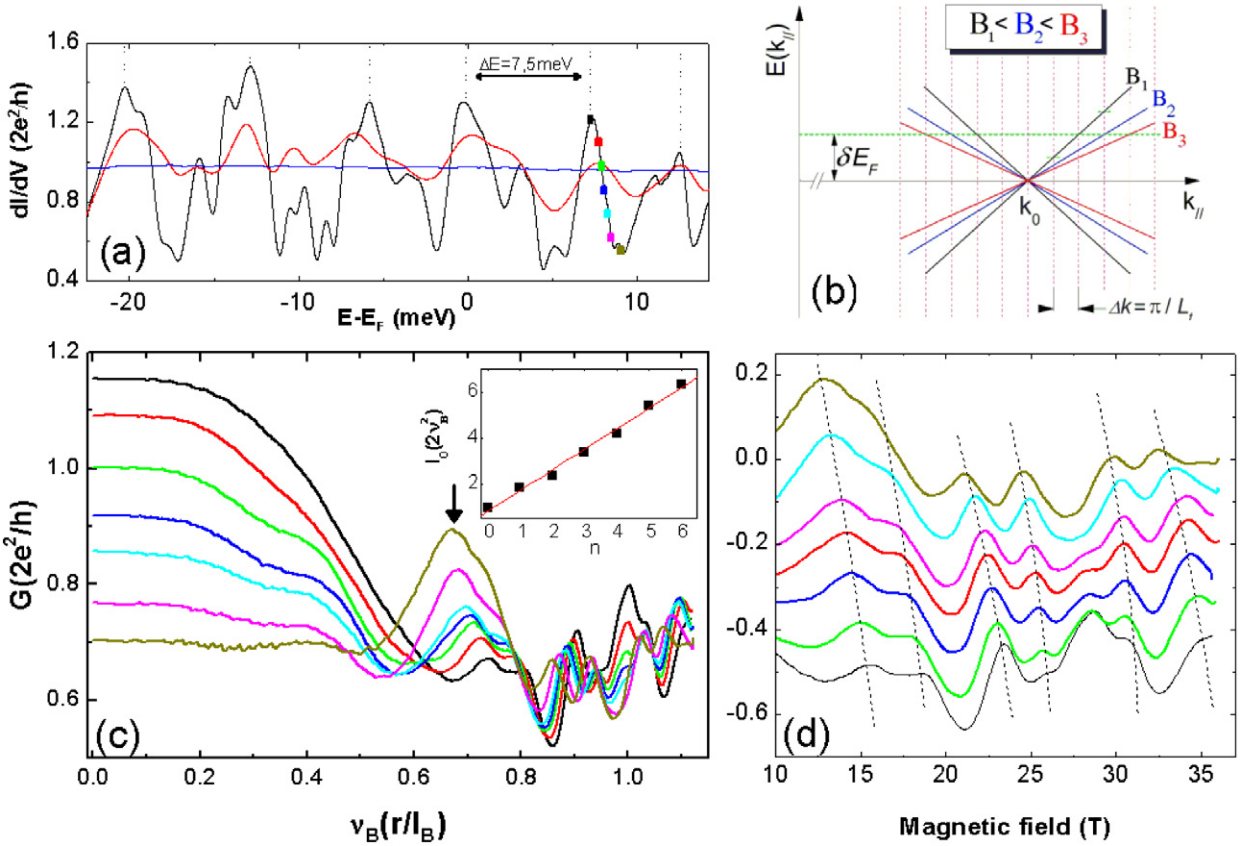

Fig. 7. (a) Conductance versus energy measured on a 10 nm diameter MWCNT at 124 K, 12 K and 2 K (respectively blue, red and black curves). Quasi-periodic oscillations, signature of Fabry–Perot interferences develop at low temperatures. (b) Illustration of the linearized dispersion relation of an armchair tube around the CNP. The onset of a Landau level under magnetic field appears with a reduced $E(k_\parallel)$ slope. B_i are the successive fields at which the resonant state of the cavity is restored. (c) Transverse magneto-conductance at 2 K in the Fabry–Perot regime, for energies indicated by color marks on (a). The arrow defines the first magnetic field induced-resonance, starting from an off-resonant state at zero field. Insert: the Bessel function $I_0(2\nu_B^2)$ calculated at each maximum of $G(B)$ at 8 meV (black curve) (d) Zoom on $\Delta G(B) = G(B) - G(B=0)$ for the same energies, the dashed lines visualize the energy-induced shifts of the modulations.

resonant state when ν_B goes beyond 0.4. Above, the conductance develops aperiodic modulations. By changing the Fermi energy by small steps of 0.3 meV, the magneto-conductance curves coherently evolve and exhibit reproducible modulations which are slightly changed in field and in magnitude (Fig. 7(d) and dashed lines to guide the eyes). Maxima (or minima) of conductance are all shifted to lower magnetic field when the Fermi energy moves away from the CNP. The average shift is of the order of $[-1.5; -0.8]$ T/meV. We argue that these results unveil the magnetic field dependence of the resonance states of the cavity. In the following, we give straightforward arguments, demonstrating that the aperiodic modulation of the electronic transmission comes from the formation of the first Landau state at the CNP. First, we consider $k_F(B) = k_F(0) + \delta k_F(B)$, the longitudinal $k_\parallel$-vectors depending on the applied magnetic field at a fixed energy E_F. Starting from a resonant state at zero field, the magnetic field successively destroys and restores the resonance of the cavity for each $\delta k_F(B) 2L_T = 2\pi n$. On the other hand, the Landau state at zero energy strongly reduces the Fermi velocity (Fig. 7(b)) and the dispersion relation is modified as follow [31,49]:

$$E_\pm(k_\parallel, \nu_B) = \pm\hbar v_F / I_0\big(2\nu_B^2\big)|k_\parallel - k_0| \tag{5}$$

where I_0 is the zeroth order modified Bessel function of the first kind and $k_0 = 8.5\ \mathrm{nm}^{-1}$. From the above expression, we infer a direct relation between the magnetic field and the successive resonant states of the cavity defined by n, at a fixed energy:

$$I_0\big(2\nu_B^2\big) = \left\{\pi n \frac{\hbar v_F / L_T}{\delta E_F} + 1\right\} \tag{6}$$

This simple model is favorably compared to the experiment. For instance, at $\delta E_F \approx 10$ meV, the cavity is in an off-resonance state at zero field. Under a magnetic field, the conductance develops a first maximum of large amplitude at $\nu \approx 0.65$ (marked by an arrow, yellow curve Fig. 7(c)). This field equals the calculated one with Eq. (6), fixing $n = \frac{1}{2}$. It corresponds to the field intensity needed to induce a first resonance of the cavity, starting from an off-state at zero field. Note that the successive resonant states driven by the magnetic field are not expected to be equidistant in field but vary as the reciprocal function of I_0. The insert of Fig. 7(c) shows the Bessel function $I_0(2\nu_B^2)$ of the resonance fields corresponding to the maxima of the magneto-conductance versus n, at 8 meV (black curve). The linear behavior as well as the slope close to unity are consistent with Eq. (6). Finally, we focus on the shift of the modulations of magneto-conductance versus the energy (Fig. 7(d)). A resonance defined by its wave vector at δE_F can be tracked by changing both the energy and the applied magnetic field. The stationary state is straightforwardly expressed by $\mathrm{d}k_\parallel = \frac{\delta k_\parallel}{\delta B}\,\mathrm{d}B + \frac{\delta k_\parallel}{\delta E}\,\mathrm{d}E = 0$. From Eq. (5), we infer the stationary condition: $\frac{\mathrm{d}B}{\mathrm{d}E} = -\frac{I_0(2\nu_B^2)}{I_1(2\nu_B^2)}\frac{1}{2\nu_B^2}\frac{B}{\delta E_F}$, where I_1 is the first order modified Bessel function of the first kind. Numerical values of the above equation give a $\mathrm{d}B/\mathrm{d}E$ slope of the order of -1 ± 0.3 T/meV, for B in the range of 10–30 T and $\delta E_F \approx 8$–10 meV, in full agreement with the experimental shift. This simple analysis captures the main features of the experimental data. A numerical calculation of the magnetic field modulation of the electronic transmission of the carbon nanotube based Fabry–Perot cavity has been developed, using the Landauer–Büttiker transport framework [53]. These simulations support the analytical model and shed light on the extreme sensitivity of the Fabry–Perot regime to unveil the magnetic field dependence of the band structure. The multiple scattering phenomena at the contacts clearly enhances the magnetic field effects and consequently unravels the early stage of the formation of the zero energy Landau state in a metallic carbon nanotube.

Complementary magneto-transport experiments have been recently performed on MWCNTs with a semi-conducting external shell [54]. We clearly observe a magnetic field induced closing of the energy gap of the semi-conducting tube with the emergence of propagative Landau states. In the high magnetic field regime, we note that metallic and semi-conducting tubes exhibit similar conductance $G(V_g)$ characteristics as predicted [31], but with an astonishing electron–hole asymmetry which remains to elucidate.

4. Conclusion and perspectives

The electronic transport properties of CNTS have been widely explored during the last decade. The use of extreme experimental conditions, like an intense magnetic field, have contributed to unveil their unique properties relaying on the band structure of graphene at the K and K' points and the tubular confinement at the nano-scale. The peculiarities of the electronic density of states and their magnetic flux dependence can be directly addressed by combining single-object transport measurements and very large magnetic fields when the magnetic length l_B becomes comparable to the radius of the tube. By playing with an applied magnetic field of few tens of Tesla parallel to the tube's axis, the drain–source conductance of a CNT-based transistor can be magnetically switched-off. While such phenomena are far from any usefulness for nano-electronics applications because of the required magnetic field intensity, its experimental evidence reveals new quantum phenomena in mesoscopic physics, i.e. the Aharonov–Bohm modulation of the band structure in the ballistic regime. In a near future, a lot remains to be explored on the current flow through individually addressed nano-objects. Among the hot topics on carbon based sp^2 nano-materials, measurements under large magnetic fields will certainly help to learn about the possible fractional Hall effect in graphene and graphite as well as the role of edge states in the graphene nano-ribbon transport properties. The merging of individual nano-objects measurements with very high magnetic fields is definitively here to last, and will for sure weigh much subsequently in nano-world exploration.

Acknowledgements

Part of this work was supported by the GDRI "Graphene and Nanotubes: Science and Applications" and EuroMagNET under the EU contract n° 228043.

References

[1] G.D.A. Jorio, G. Dresselhaus, M.S. Dresselhaus (Eds.), Carbon Nanotubes: Advanced Topics in the Synthesis, Structure, Properties and Applications, Springer, 2008.

[2] J.C. Charlier, X. Blase, S. Roche, Electronic and transport properties of nanotubes, Rev. Mod. Phys. 79 (2007) 677.
[3] H.I. Jørgensen, K. Grove-Rasmussen, T. Novitny, K. Flensberg, P.E. Lindelof, Electron transport in single-wall carbon nanotube weak links in the Fabry–Perot regime, Phys. Rev. Lett. 96 (2007) 207003.
[4] W. Liang, M. Bockrath, D. Bozovic, J.H. Hafner, M. Tinkham, H. Park, Fabry–Perot interference in a nanotube electron waveguide, Nature 411 (2001) 665.
[5] J. Nygard, D.H. Cobden, P.E. Lindelof, Kondo physics in carbon nanotubes, Nature 408 (2000) 342.
[6] P. Jarillo-Herrero, S. Sapmaz, C. Dekker, L.P. Kouwenhoven, H.S.J. van der Zant, Electron–hole symmetry in semiconducting carbon nanotube quantum dot, Nature 429 (2004) 389.
[7] P.L. McEune, M. Bockrath, D.H. Cobden, Y.-G. Yoon, S.G. Louie, Disorder, pseudospins and backscattering in carbon nanotubes, Phys. Rev. Lett. 83 (1999) 5098.
[8] H. Suzuura, T. Ando, Z. Yao, C.L. Kane, C. Dekker, Phonons and electron–phonon in carbon nanotubes, Phys. Rev. B 65 (2002) 235412.
[9] Z. Yao, C.L. Kane, C. Dekker, High field electrical transport in single-wall carbon nanotubes, Phys. Rev. Lett. 84 (2000) 2941.
[10] S. Roche, J. Jiang, L.E.F. Foa Torres, R. Saito, Charge transport in carbon nanotubes: quantum effects of electron–phonon coupling, J. Phys.: Condens. Matter 19 (2007) 183203.
[11] S. Wang, M. Grifoni, Helicity and electron-correlation effects on transport properties of double-walled carbon nanotubes, Phys. Rev. Lett. 95 (2005) 266802.
[12] F. Triozon, S. Roche, A. Rubio, D. Mayou, Electrical transport in carbon nanotubes: Role of disorder and helical symmetries, Phys. Rev. B 69 (2004) 121410.
[13] B. Bourlon, C. Miko, L. Forro, D.C. Glattli, A. Bachtold, Determination of the intershell conductance in multiwalled carbon nanotubes, Phys. Rev. Lett. 93 (2004) 176806.
[14] P. Jarillo-Herrero, J. Kong, H.S.J. van der Zant, C. Dekker, L.P. Kouwenhoven, S. de Franceschi, Electronic transport spectroscopy of carbon nanotubes in a magnetic field, Phys. Rev. Lett. 94 (2005) 156802.
[15] S. Moriyama, T. Fuse, M. Suzuki, Y. Aoyagi, K. Ishibashi, Four-electron shell structures and an intercating two-electron system in carbon nanotube quantum dots, Phys. Rev. Lett. 94 (2005) 186806.
[16] K. Kuemmeth, S. Ilani, D.C. Ralph, P.L. McEuen, Coupling of spin and orbital motion of electrons in carbon nanotubes, Nature 452 (2008) 448.
[17] B. Stojetz, C. Miko, L. Forró, Ch. Strunk, Effect of band structure on quantum interference in multiwalled carbon nanotubes, Phys. Rev. Lett. 94 (2005) 186802.
[18] B.L. Al'tshuler, A.G. Aronov, B.Z. Spivak, D.Yu. Sharvin, Yu.V. Sharvin, Observation of the Aharonov–Bohm effect in hollow metal cylinders, JETP Lett. 35 (1982) 588.
[19] R.A. Webb, S. Washburn, C.P. Umbach, R.B. Laibowitz, Observation of h/e Aharonov–Bohm oscillations in normal-metal rings, Phys. Rev. Lett. 54 (1985) 2696.
[20] S. Zaric, G.N. Ostojic, J. Kono, J. Shaver, V.C. Moore, M.S. Strano, R.H. Hauge, R.E. Smalley, X. Wei, Orbital signatures of the Aharonov–Bohm phase in single-wall carbon nanotubes, Science 304 (2004) 1129.
[21] G. Fedorov, B. Lassagne, M. Sagnes, B. Raquet, J.-M. Broto, F. Triozon, S. Roche, Gate-dependent magnetoresistance phenomena in carbon nanotubes, Phys. Rev. Lett. 94 (2005) 066801.
[22] R.C. Ashoori, Electrons in artificial atoms, Nature 379 (1996) 413.
[23] D. Vignolles, D. Smirnov, G. Rikken, B. Raquet, H. Rakoto, C. Proust, M. Nardone, J. Léotin, F. Lecouturier, M. Goiran, O. Drachenko, J.M. Broto, L. Brossard, A. Audouard, Low Temperature Physics at the Laboratoire National des Champs Magnétiques Pulsés in Toulouse, J. Low Temp. Phys. 131 (2003) 97.
[24] R. Kubo, The fluctuation–dissipation theorem, Rep. Prog. Phys. 29 (1966) 255.
[25] A. Fujiwara, K. Tomiyama, H. Suematsu, M. Yumura, K. Uchida, Quantum interference of electrons in multiwall carbon nanotubes, Phys. Rev. B 60 (1999) 13492.
[26] J.O. Lee, J.-R. Kim, J.-J. Kim, J. Kim, N. Kim, J.W. Park, K.-H. Yoo, K.-H. Park, Magnetoresistance and differential conductance in multiwalled carbon nanotubes, Phys. Rev. B 61 (2000) 16362.
[27] C. Schönenberger, A. Bachtold, Comment on magnetoresistance and differential conductance in multiwalled carbon nanotubes, Phys. Rev. B 64 (2001) 157401.
[28] A. Bachtold, Ch. Strunk, J.-P. Salvetat, J.-M. Bonard, L. Forró, T. Nussbaumer, Ch. Schönenberger, Aharonov–Bohm oscillations in carbon nanotubes, Nature 397 (1999) 673.
[29] A.G. Aronov, Yu.V. Sharvin, Magnetic flux effects in disordered conductors, Rev. Mod. Phys. 59 (1987) 755.
[30] J.-M. Bonard, T. Stora, J.-P. Salvetat, F. Maier, T. Stockli, C. Duschl, L. Forro, W.A. de Heer, A. Chatelain, Purification and size-selection of carbon nanotubes, Adv. Mater. 9 (1997) 827.
[31] H. Ajiki, T. Ando, Electronic states of carbon nanotubes, J. Phys. Soc. Jpn. 62 (1993) 1255.
[32] H. Ajiki, T. Ando, Energy bands of carbon nanotubes in magnetic fields, J. Phys. Soc. Jpn. 65 (1996) 505.
[33] Y. Aharonov, D. Bohm, Significance of electromagnetic potentials in the quantum theory, Phys. Rev. 115 (1959) 485.
[34] S. Roche, G. Dresselhaus, M.S. Dresselhaus, R. Saito, Aharonov–Bohm spectral features and coherence lengths in carbon nanotubes, Phys. Rev. B 62 (2000) 16092.
[35] F.L. Shyu, C.P. Chang, R.B. Chen, C.W. Chiu, M.F. Lin, Magnetoelectronic and optical properties of carbon nanotubes, Phys. Rev. B 67 (2003) 045405.
[36] U.C. Coskun, T.-C. Wei, S. Vishveshwara, P.-M. Goldbart, A. Bezryadin, h/e magnetic flux modulation of the energy gap in nanotube quantum dots, Science 304 (2004) 1132.
[37] J. Cao, Q. Wang, M. Rolandi, H. Dai, Aharonov–Bohm interference and beating in single-walled carbon nanotube interferometers, Phys. Rev. Lett. 93 (2004) 216803.

[38] B. Lassagne, J.-P. Cleuziou, S. Nanot, W. Escoffier, R. Avriller, S. Roche, L. Forró, B. Raquet, J.-M. Broto, Aharonov–Bohm conductance modulation in ballistic carbon nanotubes, Phys. Rev. Lett. 98 (2007) 176802.
[39] V. Derycke, R. Martel, J. Appenzeller, Ph. Avouris, Controlling doping and carrier injection in carbon nanotube transistors, Appl. Phys. Lett. 80 (2002) 2773.
[40] G. Fedorov, A. Tselev, D. Jimenez, S. Latil, N.G. Kalugin, P. Barbara, D. Smirnov, S. Roche, Magnetically induced field effect in carbon nanotube devices, Nano Lett. 7 (2007) 960.
[41] S. Heinze, J. Tersoff, R. Martel, V. Derycke, J. Appenzeller, Ph. Avouris, Carbon nanotubes as Schottky barrier transistors, Phys. Rev. Lett. 89 (2002) 106801.
[42] C. Strunk, B. Stojetz, S. Roche, Quantum interference in multiwall carbon nanotubes, Semicond. Sci. Technol. 21 (2006) S38.
[43] E.D. Minot, Y. Yaish, V. Sazonova, P.L. McEuen, Determination of electron orbital magnetic moments in carbon nanotubes, Nature 428 (2004) 536.
[44] S. Datta, Electronic Transport in Mesoscopic System, Cambridge University Press, 1998.
[45] K.S. Novoselov, A.K. Geim, S.V. Morozov, D. Jiang, M.I. Katsnelson, I.V. Grigorieva, S.D. Dubonos, A.A. Firsov, Two-dimensional gas of massless Dirac fermions in graphene, Nature 438 (2005) 197.
[46] Y. Zhang, Y.-W. Tan, H.L. Stormer, P. Kim, Experimental observation of the quantum Hall effect and Berry's phase in graphene, Nature 438 (2005) 201.
[47] E. Perfetto, J. Gonzalez, F. Guinea, S. Bellucci, P. Onorato, Quantum Hall effect in carbon nanotubes and curved graphene strips, Phys. Rev. B 76 (2007) 125430.
[48] R. Saito, G. Dresselhaus, M.S. Dresselhaus, Magnetic energy bands of carbon nanotubes, Phys. Rev. B 50 (1994) 14698.
[49] H.-W. Lee, D.S. Novikov, Supersymmetry in carbon nanotubes in a transverse magnetic field, Phys. Rev. B 68 (2003) 155402.
[50] N. Nemec, G. Cuniberti, Hofstadter butterflies of carbon nanotubes: pseudofractality of the magnetoelectronic spectrum, Phys. Rev. B 74 (2006) 165411.
[51] R. Avriller, S. Roche, F. Triozon, X. Blase, S. Latil, Low dimensional quantum transport properties of chemically disordered carbon nanotubes: from weak to strong localisation regimes, Mod. Phys. Lett. B 21 (2007) 1955.
[52] R. Avriller, S. Latil, F. Triozon, X. Blase, S. Roche, Chemical disorder strength in carbon nanotubes: magnetic tuning of quantum transport regimes, Phys. Rev. B 74 (2006) 121406(R).
[53] B. Raquet, R. Avriller, B. Lassagne, S. Nanot, W. Escoffier, J.-M. Broto, S. Roche, Onset of the Landau level formation in carbon nanotubes-based electronic Fabry–Perot resonators, Phys. Rev. Lett. 101 (2008) 046803.
[54] S. Nanot, R. Avriller, W. Escoffier, J.-M. Broto, S. Roche, B. Raquet, Propagative Landau states in multiwall carbon nanotubes, submitted for publication.